Contents lists available at ScienceDirect

Heliyon

journal homepage: www.cell.com/heliyon

Research article

Automatic computation of bone defective volume from tomographic images

M. Ezzahmouly [a,c,*], A. Essakhi [b], A. El Ouahli [c], H. El Byad [a,c], M. Ed-dhahraouy [a], S. Hakim [a], E. Gourri [c], A. ELmoutaouakkil [a], Z. Hatim [c]

[a] Research Laboratory in Optimization, Emerging Systems, Networks and Imaging, LAROSERI, Computer Science Department, Faculty of Sciences, University Chouaib Doukkali, El Jadida, Morocco
[b] Laboratory of Renewable Energy and Systems Dynamics, Faculty of Sciences Ain Chok, Casablanca, Morocco
[c] Energy, Materials and Environment Team, Chemistry Department, Faculty of Sciences, University Chouaib Doukkali, El Jadida, Morocco

ARTICLE INFO

ABSTRACT

One of the most difficult aims of modern biomaterial science is predicting the shape and volume of a bone defect and adjusting the implementation of a bone substitute. Prior to implantation, practitioners must carefully identify the architecture and volume of the defective bone to be filled. This information is often accessed via imaging techniques. The defective bone is frequently confused with its surroundings and the image background. The use of conventional segmentation for the selection and isolation of the cavity to be filled proves to be difficult. In this work, a defect in a dead bone is created and then imaged with the microtomography technique (343 cuts generated). The goal is to separate the defect's shape and volume from both the bone and the background image. An adaptive morphological operation technique was employed to complete these tasks. The proposed method allows for exact segmentation and calculation of the volume of the cavity to be filled. Using several calculated phantoms, the approach is subjectively and quantitatively evaluated: Compared to the high error value of the conventional method, the error value of the proposed one has no bearing on the overall data. The method's accuracy was also confirmed by comparing the calculated volume of the bone defect (0.91 cm^3) and the volume of prepared calcium phosphate cement paste necessary for its filling (0.87 cm^3). To challenge the method even further, another direct application on a mandibular bone is realized with an advanced number of cuts (1236 cuts). The result of this application proved that the proposed algorithm overcomes the performance of the classical approaches of segmentation with a gain of 2 min on average. A comparison study between the proposed method and other classical segmentation approaches is also presented. The effectiveness of the method is proved by the various reports and metrics generated.

The automated procedure can be beneficial in implantology for realizing and guiding surgical acts, as well as in computer-aided scaffolding techniques.

1. Introduction

For orthopedic, craniomaxillofacial, and reconstructive surgeons, large bone defects resulting from traumatic accidents, infection, or cancer resections provide a significant problem [1, 2]. For bone defect reconstruction, various techniques have been utilized in the past, including bone grafting (autografts and allografts) and the implantation of biomaterials (natural and synthetic materials) [3]. The early osseointegration of bone implants is linked to their long-term therapeutic success [4]. The stability of the implant is mostly determined by achieving the best possible contact between the bone and the implanted material [5, 6]. Predicting the shape and volume of the cavity to be filled can aid in

successful implantation [7]. CT and MRI scans are examples of imaging techniques. They enable the observation of the bone location as well as the determination of the implant's 3D model. Imaging techniques are the most effective tools for adjusting implant location and can aid the practitioner during the procedure [8]. In this context, X-ray tomography is now widely regarded as the best instrument for customized implantation. In most X-ray images, the empty volume of bone is mistaken with the background image, making traditional segmentation impossible to employ. As a result, an automatic segmentation method that recognizes the full cavity while separating it from its surroundings is required.

An open defect in a dead calf bone is produced and studied using the X-ray micro tomography technology in this study. An adaptive technique
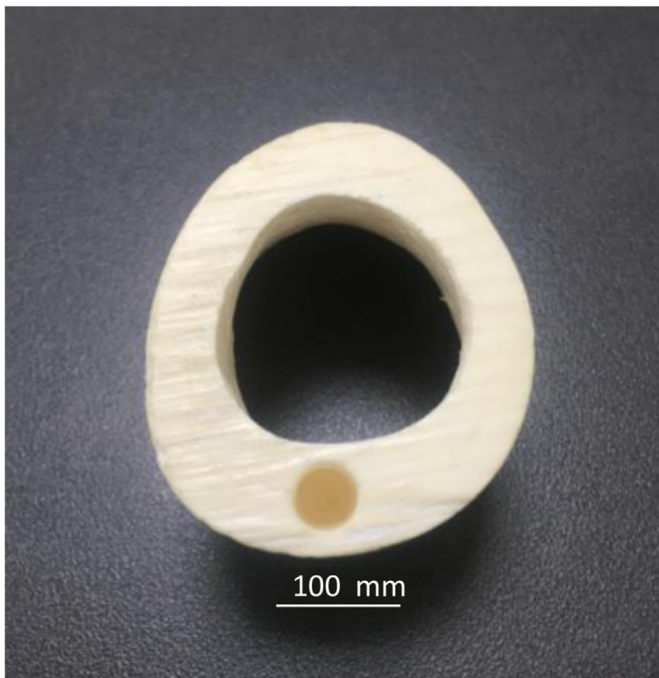

Figure 1. Photography of the bone sample with an induced defect.

based on the morphological operation algorithm was developed to quantify the produced cavity volume. This allowed us to segment the hollow, segregate it from its surroundings, and calculate various morphological metrics. The approach is tested using numerous computed phantoms. To validate the proposed method, the induced bone defect was filled with synthetic biomaterial cement. The amount of the used cement was estimated from the calculated volume. The location and the integration of the implant in the bone defect have been evaluated. The efficiency of the method was demonstrated by comparing the volume of the empty defect with the volume of the implanted cement, determined after its extraction from the bone defect. A comparison study between the proposed method and other classical segmentation approaches was also presented. Another direct application of a mandibular bone was realized with an advanced number of cuts in order to challenge the method even further.

2. Materials and methods

2.1. Preparation of a defected bone sample

In the cortical dead cattle bone, a hole was bored. Because the bone has both a mineral and an organic phase, the initial treatment is to remove the organic part (collagen and lipids), which causes the bone to
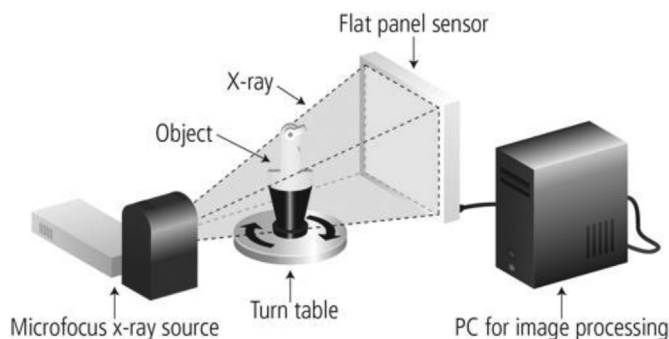

Figure 2. Illustrated principle of tomography.

Figure 3. Reconstruction process of a digital image.

deteriorate. Cleaning with appropriate solvents was used to remove organic parts while maintaining bone integrity [9]. The image of the bone with the created defect after chemical treatment is shown in Figure 1.

2.2. Imaging techniques

The biological reactions of a biomaterial implant are determined by its stability and three-dimensional architecture in the bone defect: the implant's volume should be adequate, and the implant's contacts with the recipient bone should be close.

X-ray tomography is now widely regarded as the most accurate method for determining the architecture of bone abnormalities and adjusting implant placement. This method aids the practitioner in achieving effective implantation [10].

CT (X-ray Computed Tomography) is a non-destructive method of seeing inner aspects of solid things and obtaining digital data on their 3-D geometries and properties. A slice is a common name for a CT image.

Tomographic imaging is the process of aiming X-rays towards an item from various angles and detecting the intensity drop along the way. Beer's Law, which explains intensity reduction as a function of X-ray energy, travel length, and material linear attenuation coefficient, describes this decline.

The absorption of light is therefore related to the material through which the light flows, according to Beer-law. Lambert's Similarly, the following equation (Jackson & Hawkes, 1980) (Eq. (1)) relates the absorption of x-rays to the substance through which the beam passes.

$$I = I_0 \exp(-\mu t) \tag{1}$$

where I = intensity of transmitted X-rays.

I_0 = intensity of incident X-rays

μ = material's linear attenuation coefficient

t = thickness of material through which X-rays have passed [11, 12].

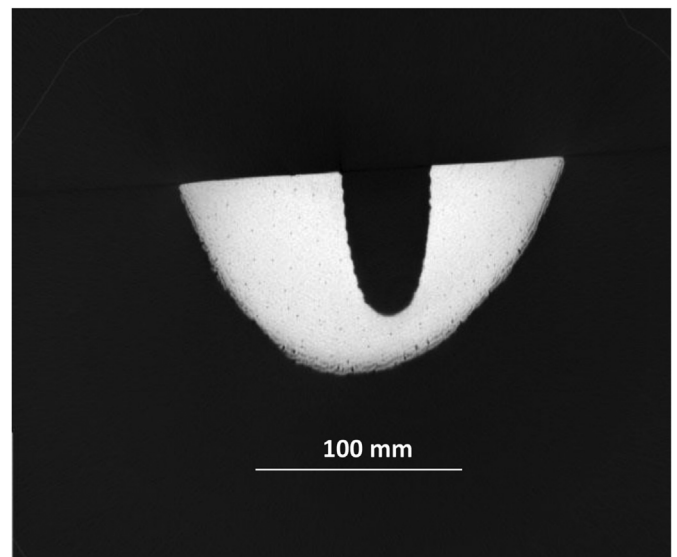The principle of tomography is depicted in Figure 2.

Figure 4. Microtomographic slice image of the defected bone that has been induced.

An algorithm is used to rebuild the distribution of X-ray attenuation in the imaged volume. Image reconstruction is the method of processing the scan data set to create an image. The image is made up of a pixel matrix and it is considered as a digital image. The image processing algorithm filtered back projection is used in CT to create or "reconstruct" the picture. The principle of image reconstruction is depicted in Figure 3. Converting the digital image into a visible and presented analog image (shades of gray) is the final step [13, 14].

As a result of changes in X-ray absorption, tomography allows access to the heart of the biomaterial to analyze the microstructure of the implant and the bone/implant contact zones. This method also allows you to see the shape and volume of the cavity to be filled, as well as the implant's incorporation into the bone.

In this study, we used a high-resolution computed microtomography (CT) instrument (EasyTom XL pair (2 sources) to examine the defective bone. Under the given conditions, the pixel size was calculated to be 33.51 m: 250 mA at 90 kV. A total of 343 cuts were made. XAct (RX solution) software was used to process the recovered images. A slice of the generated bone defect is shown in Figure 4. A proposed image processing method will then be used to calculate the defective hole.

2.3. Description of the proposed image processing method

A basic segmentation is ineffective for extracting and calculating the volume of the hole since the vacuum is coupled to the background image in this scenario (Figure 4). We apply an adaptive strategy based on the morphological operation algorithm to solve this problem. The goal of our image analysis method is to distinguish the bone cavity volume from its surroundings.

First, we'll go through the preprocessing process. The non-local mean (NLM) filter is employed. In contrast to "local mean" filters, which smooth the image by taking the mean value of a group of pixels around a target pixel, non-local means filtering takes the mean of all pixels in the image, weighted by how similar these pixels are to the target pixel. This leads in significantly higher post-filtering clarity and less loss of detail in the image as compared to local mean approaches [15].

The estimated value $NL[v](i)$ for a pixel i is derived as a weighted average of all the pixels in the image (Eq. (2)), given a discrete noisy image $v = \{v(i) \mid i \in I\}$,

$$NL[v](i) = \sum_{j \in I} w(i, j)v(j), \tag{2}$$

where the $\{w(i, j)\}_j$ family of weights is based on the similarity of the pixels i and j and meets the standard conditions $0 \leq w(i, j) \leq 1$ and $\sum_j w(i, j) = 1$ [16].

The threshold is deliberately chosen to separate the bone structure from its surroundings. It converts a gray-scale image to a binary image, with the two levels allocated to pixels that are below or over a threshold value [17].

It is useful to be able to separate out the regions of the image corresponding to the bone, from the regions of the image that correspond to the rest of the sample and the background [18, 19, 20, 21]. However, the simple threshold does not allow separating the hole in which we are interested.

Several segmentation methods exist which are widely used. Among these methods, there is the mathematical morphology operation [22, 23, 24, 25].

In image processing and form analysis of aspects of interest, mathematical morphology has been widely used.

Union, intersection, and complement are the three basic morphological set operations. The original data and data translated from the original with a reference shape called a structuring element are the operands of the set operations.
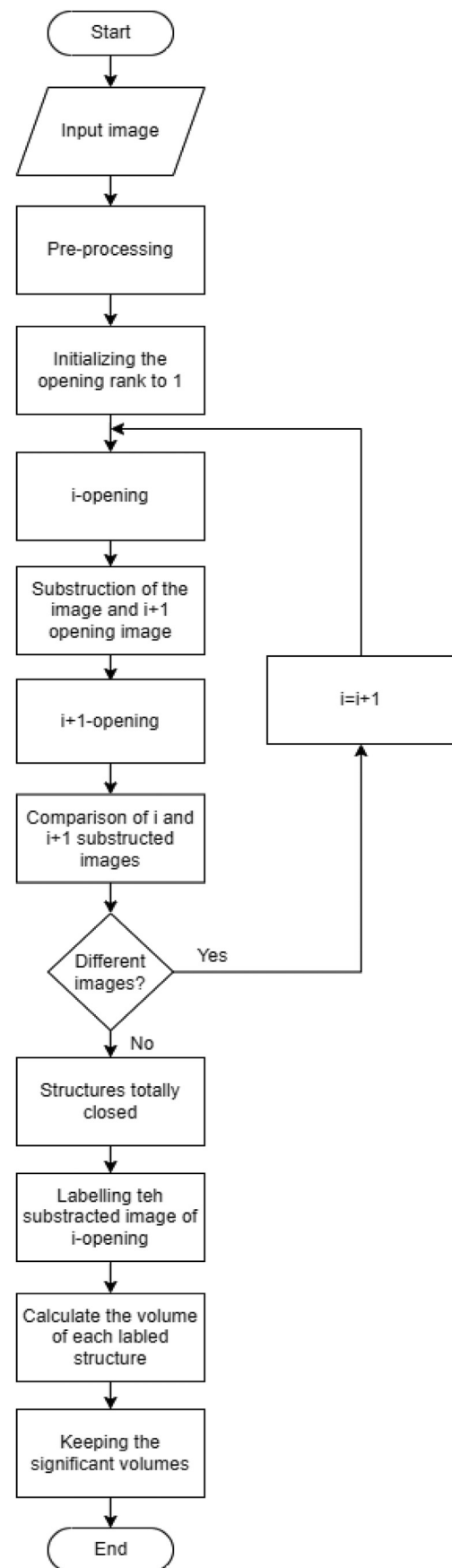

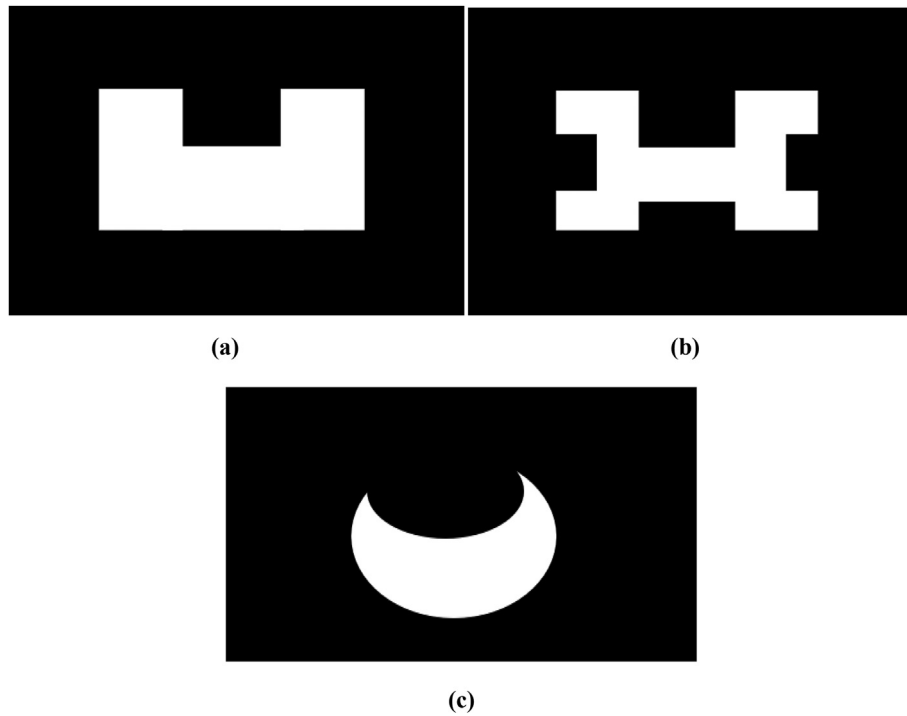**Figure 5.** Flowchart of the proposed method.

Figure 6. Phantom cases: (a)- phantom with single hole (b)- phantom with different holes and sizes (c)- phantom with a hole with an elliptical shape.

1. Calcium phosphate powder + liquid cement   **2. Moldable past of cement**   **3. Bone filling**
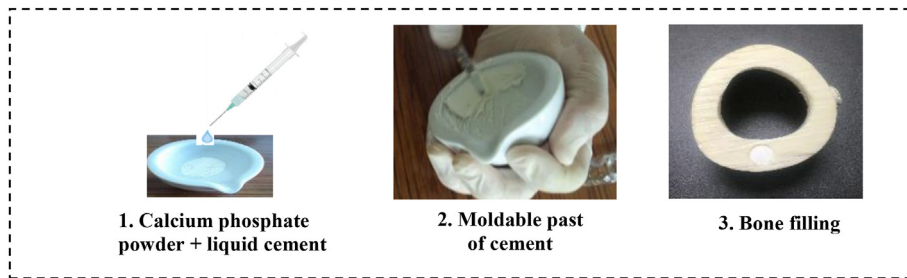
Figure 7. Steps of preparation process of a moldable paste for the bone filling.

A set of vectors can be used to create a structuring element. The basic Minkowski set operations of addition and subtraction can then be used to define the essential mathematical morphological processes of dilation and erosion.

Erosion and dilation are mathematical morphology tools that allow us to add or subtract pixels from objects in an image based on the size and shape of the structuring element used to process the image.

The set operation (Eq. (3)) describes the erosion of image I by a structure element H.

$$I\Theta H = \left\{p \in Z^2 \,\middle|\, (p+q) \in I, \text{ for every } q \in H\right\} = \bigcap_{q \in H} I_{-q} \tag{3}$$

The set operation (Eq. (4)) is used to dilate an image I by a structure element H.

$$I \oplus H = \left\{(p+q) \,\middle|\, p \in I, \; q \in H\right\} = \bigcup_{p \in I} H_p = \bigcup_{q \in H} I_q \tag{4}$$

Holes in the foreground those are smaller than H will be filled.

Erosion reduces the size of the feature by eroding its outline, and dilatation increases the size of the feature by dilating its outline, both of which are controlled by a predetermined structure element. The process of erosion followed by dilation is known as opening. Erosion and dilation are utilized to close or open certain morphological characteristics, such as holes, in this study [26, 27, 28].

Separating the hole from the bone is helpful for efficient segmentation. This allows us to determine a variety of factors, including the hole volume and the contact surface.

For quantitative analysis, the method relying solely on openings is ineffective. This method ignores convexity hypotheses for the forms encountered and lacks an end condition to stop or continue the procedure.

To get over these limitations, we suggest a mathematical morphology extension. To gradually seal the holes, we compute repeated openings operations with structural elements increasing in diameter. The volume of the hole being closed corresponds to the difference between the image before and after an opening.

If the bone just has one hole, this approach still works. If there are numerous holes of different sizes, it is recommended that a subtraction operation be performed between the image before and after each opening process. This difference relates to the structures added to the original image by the opening operation. In other words, it corresponds to partially or completely closed open structures. To finish the total closure, we compare the subtracted image after an opening of I and an opening of I + 1 until they are the same, at which point we may claim that all of our open structures have been closed.

We label our subtracted images at this point, and we calculate the volume of each identified structure. At this point, we maintain the largest volumes, which reflect significant holes that must be filled by the

Figure 8. Photographic image of the induced defect with hard cement.

practitioner. The flowchart of the suggested approach to separate and calculate distinct hole volumes is shown in Figure 5.

2.4. Validation of the proposed method

To validate our method and vary the case studies, we proposed:

- Study on computed phantoms connected to the background.
- Direct application on the defected bone with an induced hole to fill.
- Another direct application on defected mandibular bone.

2.4.1. Phantoms and error estimation study

2.4.1.1. Features of studied phantoms. To validate our method, phantoms with shapes of different sizes are computed (Figure 6).

The phantom with a single shape (Figure 6– (a)) is utilized to demonstrate how the procedure is statistically exact and capable of maintaining the original structure's shape and volume.
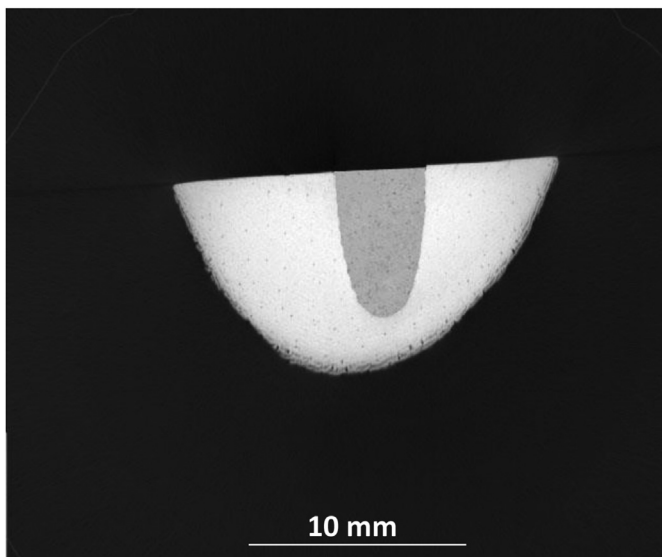

Figure 9. –Slice tomographic image of the defect bone filled with hard calcium phosphate cement.

Figure 10. Photographic image of the defected mandibular bone.

Another objective is to fill and calculate different and significant holes. Hence the choice of a phantom containing different shapes with different sizes (Figure 6– (b)) and a phantom with an elliptical shape (Figure 6– (c)).

2.4.1.2. Error estimation. To evaluate the accuracy of our method, the absolute error value of the conventional opening method and the proposed one was calculated and then the Mean Absolute Error (MAE) value was determined.

The difference between the measured and actual value is the absolute error (e). It is one way to consider an error when measuring the accuracy of values (Eq. (5)).
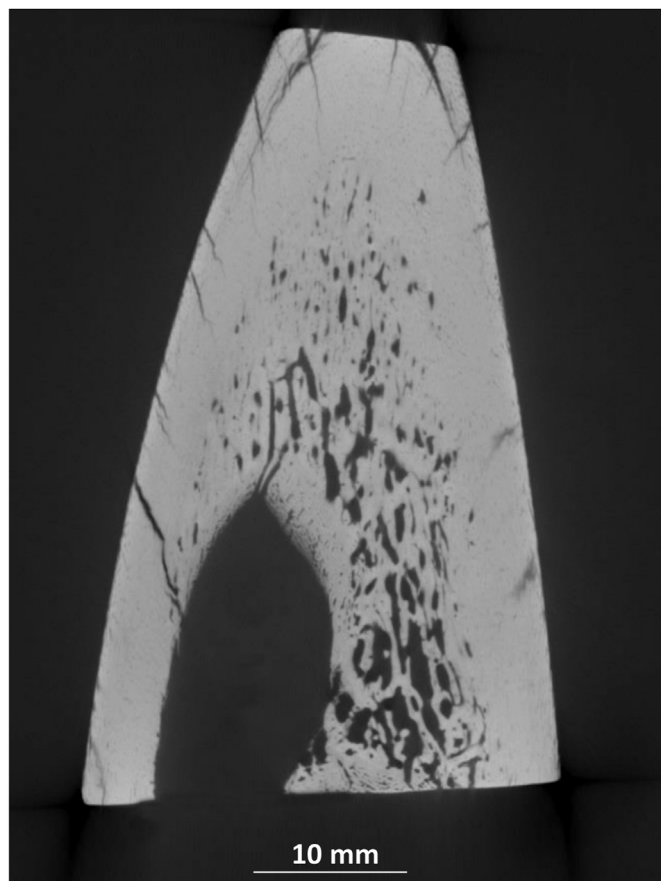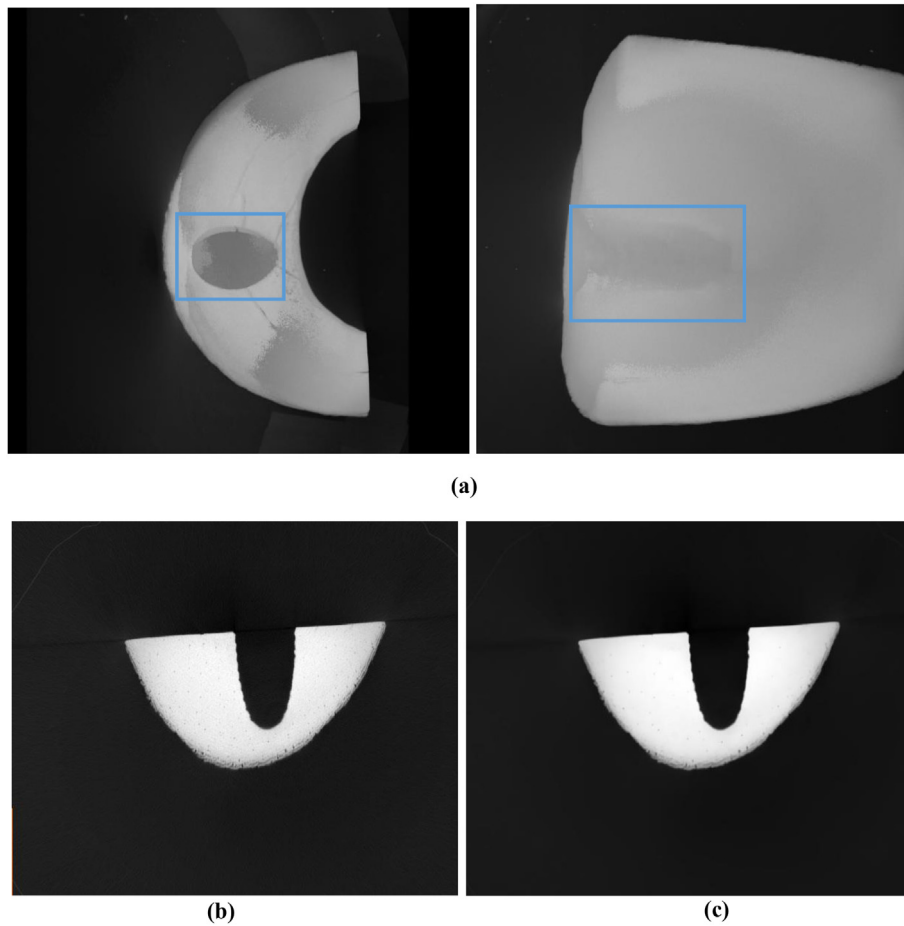

Figure 11. Slice tomographic image of the defected mandibular bone.

Figure 12. (a) 3D visualization of the bone sample, Slice of tomographic images (b) before, (c) after applying the non-local mean filter.

$$e = x_o\text{-x} \tag{5}$$

where e–the absolute error (the difference, or change, in the measured and actual value), x_o–the measured value, and x–the actual value.

Mean absolute error (MAE) is a measure of the difference between two variables. It is expressed as the following Eq. (6).

$$MAE = \sum_{i=1}^{n} \left| e_i \right| \Big/ n \tag{6}$$

where n– number of variables.

2.4.2. Filling bone defect with calcium phosphate paste

Calcium phosphates are proposed in many forms and compositions to satisfy as much as possible all applications of dentistry and orthopedics area where necessaries are the bone repair or replacement. Substitutes bone can be used in different shapes: cylinder, cube, disc, rod, block, or paste [29].

Phosphocalcic cements are biomaterials prepared in the form of paste used directly in the bone defect in order to fill it [30].

The hardening of the paste is obtained in vivo by crystallization of phosphocalcic nanomaterial. Phosphocalcic cements are known today for their bioactivity which promotes bone reconstruction [31, 32].

During our study, the accuracy of the proposed method has been verified by comparing the calculated volume of the induced defect bone and the volume of prepared calcium phosphate cement necessary for its filling.

2.4.2.1. Preparation of calcium phosphate paste.
Tetra-calcium powder ($Ca_4(PO_4)_2O$) was mixed with an aqueous solution of phosphoric acid (H_3PO_4), calcium chloride ($CaCl_2, 2H_2O$), and lactic acid ($C_3H_6O_3$) to make the cement paste [33].

The molar ratio Ca/P of the mixture was 1.63 and the liquid (L) to solid (S) ratio (L/S) was 0.55 ml g^{-1}. The prepared mixture was done manually in a mortar for 2 min. The components turn into a moldable paste which will serve to fill the induced bone defect (Figure 7).

2.4.2.2. Filling bone defect.
The prepared paste was placed in a syringe in sufficient amounts to fill the hole. The amount of cement necessary was estimated from the calculated volume. The bone with the implant was then placed in water at 37 °C for 24 h. In a humid environment, the paste placed in the bone cavity turns into calcium phosphate hard cement with a composition very close to that which composes natural bone ($Ca_{10}(PO_4)_6(OH)_2$: hydroxyapatite). Figure 8 shows a photographic image of the induced defect with hard cement. Analysis using an X-ray microcomputed tomography (µCT) can help to quantify the volume of the induced defect and the amount of calcium phosphate cement needed to fill it.

2.4.2.3. Characterization by X-ray microtomography.
The microstructure and location of hardening cement paste inside a cortical bone cavity are investigated by microtomography (µCT). Figure 9 shows a tomography slice image of the bone defect filled with hard calcium phosphate cement.

Figure 13. Tomographic slice image after applying simple threshold method.

2.4.2.4. Calculation of the volume of the empty cavity. At first, the proposed method was applied to tomographic images of the defect bone alone. Different openings are processed, with structuring element increasing in diameter until all the structures are totally closed.

After the different operations of opening, the volume of the cavity was then calculated by labeling the significant structure and calculating its volume.

The volume obtained from the empty cavity will be compared with the volume of the implant after extraction from the bone.

2.4.2.5. Extraction of the implanted cement and calculation of its volume. To separate and extract the cement from the bone defect, we perform thresholding segmentation.

Image thresholding provides an easy and convenient way to perform this segmentation based on different intensities. It isolates objects by converting grayscale images into binary ones. Thresholding is the most effective way, in our case, because we have images (bone + implant) with high levels of contrast.

The volume of the isolated implant is then calculated to compare it with the volume found for the empty cavity.

2.4.3. Other application on a defected mandibular bone

In addition to the application of the method on phantoms and on a defect-induced hole on a dead bone, another application on a mandibular bone with a hole connected to the background. The goal is to determine the empty volume in order to give an idea to the practitioner on the volume to be prepared for filling. Figure 10 shows a photographic image of the defected mandibular bone.
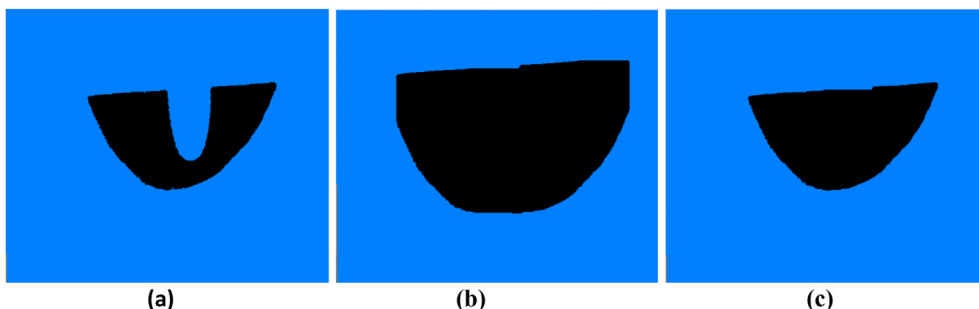
Table 1. The volume of the real computed phantoms, the conventional and the proposed method.

Phantom	Hole number	The real distribution (vx)	Conventional method (vx)	Proposed method (vx)
a	1	391620	388990	391620
b	1	391620	388990	391620
	2	192600	189150	192600
	3	151200	147530	151200
	4	131760	127520	131760
c	1	581530	574062	581530

Table 2. MAE value of the conventional and the proposed method for the computed phantoms.

	Phantom	Hole number	Conventional method	Proposed method
Mean Absolute Error (MAE)	a	1	2630	0
	b	1	2630	0
		2	3450	0
		3	3670	0
		4	4240	0
	c	1	7468	0

This defected bone was imaged with computed microtomography (μCT) a high-resolution device (EasyTom XL duo (2 sources)). The pixel size was determined at 32.64 μm under the following conditions: 70 kV, 428 mA. About 1236 cuts were generated. The reconstructed images were processed with XAct (RX solution) software. Figure 11 shows a slice of the defected mandibular bone.

For performance calculation purposes, we used this example to challenge the method in terms of execution time. Unlike the previous example with 343 cuts, this example is characterized by 1236 cuts.

3. Results and discussion

3.1. Bone defect study

3.1.1. Non-local mean filter

The tomographic images were subjected to a non-local mean filter. The 3D visualization of the bone (Figure 12-a) and a slice of the tomographic image before (Figure 12-b) and after filtering are shown in Figure 12 (Figure 12-c).

The NLM algorithm preserves edge information and images thanks to its principle that exploits image similarity - first, the similarity between similar blocks and the weighted average is used to recover the value of the pixel to be restored after calculating the image block where the present noise is located. After that, excellent structural information performance is acquired.

Non-local mean filtering provides the advantage of a constant denoising effect and no blur detail, and can better preserve edge and picture structural information when compared to other approaches.
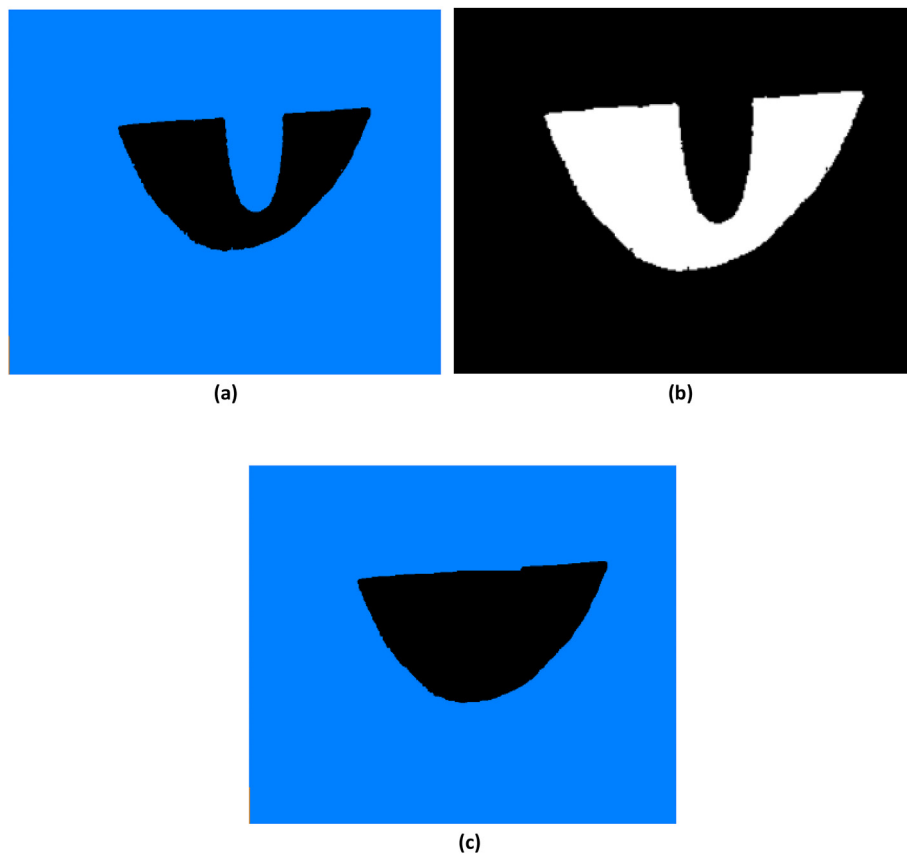

| (a) | (b) | (c) |

Figure 14. Results of the proposed method: Slice of tomographic image. (a) Pre-processing step. Application of an advanced rank of (b) erosion, (c) dilation.

Figure 15. Results of tomographic slice image of defected bone segmented after applying (a) Simple threshold (b) Otsu threshold (c) the proposed method.

3.1.2. Initial segmentation

The effect of a simple threshold applied to tomographic images is shown in Figure 12. As we can see, thresholding has limitations in terms of what it can accomplish and automatically estimating the best threshold is tough.

In fact, the thresholding method does not guarantee that the pixels it identifies are contiguous. We can readily include pixels that aren't part of the targeted zone, and we can also easily overlook isolated pixels inside the region (especially at the region's edges) (Figure 13).

Table 3. Comparison between several approaches used for segmentation.

Method	Principle	Result obtained or constraint encountered
Global threshold-Otsu	Based on the histogram, seeks to maximize the within-class variance.	Problems in this case with the presence of several classes. **V = 9.7 cm^3** (background and hole confused)
Local threshold-Bernsen & al [34]	Estimate the threshold value by averaging the highest and lowest value in the window.	The threshold is too low when the window is centered in the background. **V = 10.4 cm^3** (background and hole confused)
Local threshold-Niblack & al [35]	Taking into account the variance and the mean.	The appearance of noise in uniform areas of the image. **V = 11.2 cm^3** (background and hole confused)
Rising water-Kim & al [36]	Use pixel values as contour lines to simulate rising waters.	Difficulties in adapting the water flow or the number of iterations to the image.
Markov fields-Wolf & al [37]	Use Markov fields to find out the areas of interest.	The constants to be adjusted prevent the method from perfectly processing non-uniform images.
Growing regions- Lienhart & al [38]	Increase of regions where the borders move according to the gradient.	Practically random memory access slows down the algorithm. Execution time is too slow, estimated at more than **20 min** and background and hole are confused.
Neural networks- Caponetti & al [39]	Uses two fuzzy neural networks to segment an image.	The learning phase is very cumbersome to set up due to the type of network.
Fourier transform- Zhong & al [40]	Pass the image in the frequency domain.	Loss of localization. Requires an analysis window.
Mathematical morphological operation	Theoretical and practical aspects of geometrical structure analysis and processing.	Information loss. **V = 0.73 cm^3**
Proposed approach	The method highlights variations in the image. Fast, allows locating outlines and holes.	**V = 0.91 cm^3**

(a) **(b)**
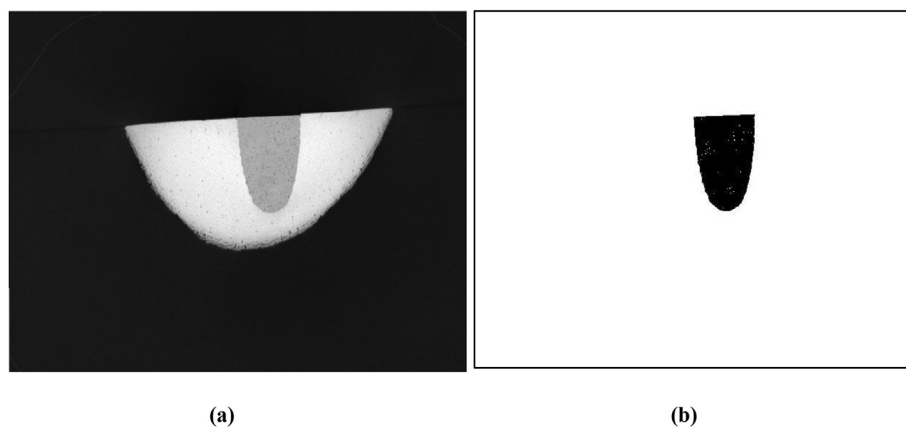
Figure 16. Tomographic slice image of (a) bone and implant (b) Calcium phosphate Implant extracted from bone tomographic image.

Traditional thresholding prevents an efficient extraction of the hole volume from the bone, which might have a negative impact on the implant procedure and data processing.

3.1.3. The proposed method's application

The tomographic images were processed utilizing the materials and methods section's approach. Following the pre-processing procedures, we erode and dilate the image until we reach the entire closed volume. The steps of the suggested operations to determine the volume of the hole to be filled are shown in Figure 14.

The process of assigning a label to the voxels sharing the same structure is performed after implementing a series of erosion and dilation (with the end condition of the loop: obtaining similar images, after the operation of subtraction, between the opening of order i and order i + 1). The volume of each named structure is computed once the vacuum has been effectively closed. Only the most significant volumes are retained at this time. 0.91 cm^3 is the calculated hole volume.

3.2. Method validation results

3.2.1. Study of phantoms and error estimation

The computed phantoms are opened using both the conventional and proposed methods. The error estimation is calculated for each of the analyzed scenarios.

Table 1 summarizes the volume distribution of the real calculated phantom as well as the results obtained using the conventional and proposed methods.

To know how reliable our method is, the error calculation method was chosen using Eqs. (4) and (5). The results are summarized in Table 2. For the error computation, the manual technique was used as a reference method.

For a low MAE value, the reliability of the method increases. Compared to the high error value of the conventional method (Table 2), the error value of the proposed one does not affect the general statistics.

The result shows that our method gives close outcomes to the real structure.

The proposed method makes it possible then to segment holes connected to the background and to define with precision the right volume of each hole.

3.2.2. Comparison between the proposed method and other approaches

Our method has been compared with several approaches. First, the classical threshold method and the Otsu method were used, then a large comparison with several methods was demonstrated.

3.2.2.1. Simple threshold, Otsu threshold and the proposed method.-
Figure 15 shows the result of the simple threshold, Otsu threshold, and proposed method applied to the tomographic images.

As we can see, simple and classical thresholding is limited in what they can achieve. For the first method, the use of empirically defined thresholds makes the method not very robust (Figure 15a) and for the second one, there are considerable difficulties in automatically estimating the optimum threshold (Figure 15b).

On the other hand, the proposed method succeeded in closing the open hole in an efficient manner (Figure 15c).

3.2.2.1. Proposed method vs other approaches. There are many methods of segmentation. We have chosen a few of the most widespread and used them to compare with our method using the tomographic images of the sample (Figure 4). Table 3 summarizes the result of this comparison by presenting the general principle of each method, the result obtained, or the difficulty encountered during its use.

The disadvantage of the previous methods is of the same type as classical and Otsu threshold binarization: it is too general to adapt to images with specific characteristics. As with binarization, research then turned to adaptive methods on which our method is based.

3.2.3. Bone/implant study

To validate our method and evaluate the results of the calculated volume of the empty cavity, an adequate quantity of implant was used for its filling. Bone and implant were then analyzed by microtomography. The image shows the perfect and total integration of the cement in the bone structure (Figure 16a). Extraction of the implant from the bone structure is then performed. The result obtained is shown in Figure 16 b. By applying the proposed algorithm, the calculated volume of the extracted implant is about 0.87 cm^3 slightly less than the calculated cavity volume (0.91 cm^3).

3.2.4. Mandibular bone study

After presenting the results related to the study of phantoms and the study on the defective compact bone, we proceed to expose the result of the direct application of the proposed method on the defective mandibular bone. The outputs of the method are numerous due to the fact that in this application, the microstructure of the bone is different. We then obtain several volumes classified according to the largest to the smallest however only the significant volume is designated. The volume value is estimated then to 2.73 cm^3.

We also note an execution time of almost 2 min for 1236 cuts against 4 min of treatment using a conventional segmentation method.

By using a parallel processing approach, we can save a lot of processing time and then the number of cuts does not really impact the performance of the method.

In summary, we used an adaptive morphological operation technique to segment the volume of the bone defect from the bone structure and the background of a micro-tomographic picture. The proposed approach is a series of openings processes based on the morphological operation algorithm for closing holes and determining morphological parameters. The method has the advantages of threshold-based methods in terms of speed and simplicity, and it eliminates background noise and improves tomographic image contrast. We extract geometric information from the images after executing the morphological procedure. As a result, the relevant qualities, such as the open limit with respect to the external environment, are chosen.

Unlike the conventional threshold, our method detects the shape of the cavity during the computation by isolating it from both the bone and the background image, providing for precise measurement of the volume of the hole to be filled. By comparing the results of the standard approach's segmentation with those of the suggested method, it was demonstrated that our method effectively closed the vacuum. As a result, the proposed solution solves the threshold method's shortcomings.

To evaluate our method, the induced bone defect was filled by a biomaterial in the form of a paste in situ hardening. The amount of the past was estimated from the calculated volume.

The location of the implant in the bone defect has been evaluated using the x-ray scanner technique. The perfect integration of cement into the defect has been observed. The proposed method allowed us to calculate different morphological parameters, segment, isolate and extracted the implant and calculate its volume. The results show that the value calculated for the volume of the defect bone and the volume of the extracted cement are very close. The proposed method, therefore; ensures precise control of the filling of the empty cavity.

The automatic process, proposed in this work, can be used favorably in computer processing of medical images, particularly in the field of bone tissue engineering. It can be used to isolate the geometrical configuration of the bone defect and in the design and control of prefabricated three-dimensional structures [41]. After the chirurgical act, the proposed method can also be used to follow up on the integration of the implant and regenerated bone.

4. Conclusion

In implantology, imaging techniques are the most appropriate tools for the adjusted placement of bone implants. Segmentation of images is typically used to locate objects and boundaries. This study provides an automatic process based on the morphological operation algorithm to segment images obtained from the micro tomograph. The proposed method lets to segment, isolate the geometrical disposition of bone defect and calculate precisely its volume. The method was evaluated by using computed phantoms. The good performance of the proposed method was demonstrated by comparing the result of structure distribution with the conventional one. The method's accuracy was also confirmed by comparing the calculated volume of the bone deficiency to the volume of synthetic biomaterials required to fill it. The proposed method, therefore, overcomes the poor performance of the threshold method. Moreover, a comparison with standard segmentation methods has been established which has shown that our approach gives satisfactory results. To challenge the method even further, another direct application of a mandibular bone was realized with an advanced number of cuts. The result of this application demonstrated the good performance and optimum execution time of our method thanks to the parallel processing carried out.

The automatic process can be considered as an important tool for the adaptation of implant in a 3D environment allowing new perspectives in the design and control of substitutes for tissue regeneration and in order to facilitate the surgical act.

Declarations

Data availability statement

Data will be made available on request.

Declaration of interests statement

The authors declare no conflict of interest.

Additional information

No additional information is available for this paper.

References

[1] R.L. Huang, E. Kobayashi, K. Liu, Q. Lia, Bone graft prefabrication following the in vivo bioreactor principle, EBioMedicine 12 (September 2016) 43–54.

[2] E. Guerado, E. Caso, Challenges of bone tissue engineering in orthopaedic patients, World J. Orthoped. 8 (2) (February 2017) 87–98.

[3] M. Ansari, Bone tissue regeneration: biology, strategies and interface studies, Prog. Biomater. 8 (2019) 223–237. November 2019.

[4] J.T. Steigenga, K. Al-Shammari, F.H. Nociti, C.E. Misch, Dental implant design and its relationship to long-term implant success, Implant Dent. 12 (4) (February 2003) 306–317.

[5] S. Parithimarkalaignan, T.V. Padmanabhancorresponding, Osseointegration: an update, J. Indian Prosthodont. Soc. 13 (1) (January 2013) 2–6.

[6] M. Ezzahmouly, A. Elmoutaouakkil, M. Ed-Dhahraouy, H. Khallok, A. Elouahli, A. Mazurier, A. ElAlbani, Z. Hatim, Micro-computed tomographic and SEM study of porous bioceramics using an adaptive method based on the mathematical morphological operations, Heliyon 5 (12) (December 2019).

[7] Ca.N. Elias, Factors Affecting the Success of Dental Implants, Intech Open, 2011.

[8] X. Gao, M. Fraulob, G. Haïat, Biomechanical behaviours of the bone–implant interface: a review, Royal. Soc. 16 (July 2019) 156.

[9] S. Gupta, N. Patil, J. Solanki, R. Singh, S. Laller, Oral implant imaging: a review, Malays. J. Med. Sci. 22 (3) (May-June 2015) 7–17.

[10] P.M. Charlene, B. Bujoli, E. Guilminot, G. Lemoine, Analysis of fatty acids extracted from a whale skeleton: analytical approach to evaluate the efficacy of degreasing treatment, J. Am. Inst. Conserv. 54 (3) (August 2015) 168–180.

[11] A. Nagarajan, R. Perumalsamy, R. Thyagarajan, ANamasivayam, Diagnostic imaging for dental implant therapy, J. Clin. Imag. Sci. 4 (Suppl 2) (October 2014) 4.

[12] S. Kelkar, C.J. Boushey, M. Okos, A method to determine the density of foods using X-ray imaging, J. Food Eng. 159 (August 2015) 36–41.

[13] E. Seeram, Computed tomography: physical principles and recent technical advances, J. Med. Imag. Radiat. Sci. 41 (2) (June 2010) 87–109.

[14] M.J. Willemink, P.B. Noël, The evolution of image reconstruction for CT—from filtered back projection to artificial intelligence, Eur. Radiol. 29 (2019) 2185–2195.

[15] A.-F. Obaton, J. Fain, M. Djemaï, D. Meinel, F. Léonard, E. Mahé, B. Lécuelle, J.-J. Fouchet, G. Bruno, In vivo XCT bone characterization of lattice structured implants fabricated by additive manufacturing, Heliyon 3 (8) (August 03, 2017).

[16] R. Brad Abrahams, W. Huda, W.F. Sensakovic, Imaging Physics Case Review E-Book, Elsevier Health Sciences, March 2019.

[17] M.N. Favorskaya, L.C. Jain, Computer Vision in Advanced Control Systems-5: Advanced Decisions in Technical and Medical Applications, Springer, December, 2019.

[18] N. Otsu, A threshold selection method from gray-level histograms, IEEE Trans. Sys. Man. Cyber. 9 (1) (1979) 62–66.

[19] K. Byung-Gyu, S. Jae-Ick, P. Dong-Jo, Fast image segmentation based on multi-resolution analysis and wavelets, Pattern Recogn. Lett. 24 (15) (2003) 29953006. Elsevier.

[20] H. Deng-Yuan, W. Chia-Hung, Optimal multi-level thresholding using a two-stage Otsu optimization approach, Pattern Recogn. Lett. 30 (3) (2009) 275–284.

[21] L. Ping-Sung, C. Tse-Sheng, C. Pau-Choo, A fast algorithm for multilevel thresholding, J. Inf. Sci. Eng. 17 (5) (2019) 713–727.

[22] P.P. Roy, U. Pal, J. Lladós, F. Kimura, Convex hull based approach for multi-oriented character recognition from graphical documents, in: 19th international conference on pattern recognition, 2009, pp. 1–4.

[23] K.C. Santosh, P.P. Roy, Arrow detection in biomedical images using sequential classifier, Int. J. Mach. Learn. Cybernet. 9 (6) (2018) 993–1006.

[24] S. Gupta, P.P. Roy, D.P. Dogra, B.G. Kim, Retrieval of colour and texture images using local directional peak valley binary pattern, Pattern Anal. Appl. 23 (4) (2020) 1569–1585.

[25] S. Mukherjee, P. Kumar, R. Saini, P.P. Roy, D.P. Dogra, B.G. Kim, Plant disease identification using deep neural networks, J. Multimedia Inform. Syst. 4 (4) (2017) 233–238.

[26] A. Buades, B. Coll, J.M. Morel, A non-local algorithm for image denoising, in: IEEE Computer Society Conference on Computer Vision and Pattern Recognition (CVPR'05). San Diego, CA, USA, vol. 2, July 2005, pp. 60–65.

[27] O.D. Faugeras, Fundamentals in Computer Vision: an Advanced Course, CUP Archive, July 1983.

[28] Y. Kimori, Morphological image processing for quantitative shape analysis of biomedical structures: effective contrast enhancement, J. Synchrotr. Radiat. 20 (Pt 6) (2013 Nov 1) 848–853.

[29] S.V. Dorozhkin, Dental applications of calcium orthophosphates (CaPO4), J. Dent. Res. 1 (2019) 1007.

[30] L. Leroux, Z. Hatim, M. Freche, J.L. Lacout, Effects of various adjuvants (lactic acid, glycerol and chitosan) on the injectability of a calcium phosphate cement, Bone 25 (1990) 31S–34S.

[31] S.V. Dorozhkin, Self-setting calcium orthophosphate (CaPO4) formulations and their biomedical applications, AdvNanoBioM&D 3 (3) (2019) 321–421.

[32] J.P. Schmitz, J.O. Hollinger, S.B. Milan, Reconstruction of bone using calcium phosphate bone cements: a critical review, J. Oral Maxillofac. Surg. 57 (1999) 1122–1126.

[33] Z. Hatim, El.H. Gourri, A. Kheribech, Procédé de préparation d'un ciment phosphocalcique à usage orthopédique et odontologique, Patents (MA 32913 B1), 1999.

[34] J. Bernsen, Dynamic thresholding of grey-level images, in: Proc. Eighth Int ́l Conf. On Pattern Recognition, 1986, pp. 1251–1255.

[35] W. Niblack, An introduction to digital image processing, Prent. Hall 1986 (July 1986).

[36] I.-K. Kim, D.-W. Jung, R.-H. Park, Document image binarization based on topographic analysis using a water flow model, Pattern Recogn. 35 (2002) 265–277.

[37] C. Wolf, D. Doermann, Binarization of low quality text using a markov random field model, in: Proceedings of the 16 th International Conference on Pattern Recognition (ICPR'02), vol. 3, 2002, p. 30160.

[38] R. Lienhart, W. Effelsberg, Automatic text segmentation and text recognition for video indexing, Multimed. Syst. 8 (2000) 69–81.

[39] L. Caponetti, C. Castiello, P. Gorecki, Document page segmentation using neurofuzzy approach, Appl. Soft Comput. 8 (2008) 118–126.

[40] Y. Zhong, H. Zhang, A.K. Jain, Automatic caption localisation in compressed video, IEEE Trans. Pattern Anal. Mach. Intell. 22 (4) (2000) 385–392.

[41] M. Ezzahmouly, A. ELmoutaouakkil, M. Ed-dhahraouy, S. Hakim, H. El Byad, E. Gourri, Z. Hatim, Development of an automatic process for calculation of bone defected volume from tomographic images, in: Advances in Intelligent Systems and Computing Book Series (AISC, Volume 1418), 10 February 2022.